Lectin-Recognizable Colloidal Dispersions Stabilized by *n*-Dodecyl β-D-Maltoside: Particle−Particle and Particle−Surface Interactions

Woo-Sung Bae and Marek W. Urban*

School of Polymers and High Performance Materials, Shelby F. Thames Polymer Science Research Center, The University of Southern Mississippi, Hattiesburg, Mississippi 39406

Received December 20, 2005; Revised Manuscript Received January 27, 2006

Recently, we reported that it is possible to utilize sugars as stabilizing agents for colloidal particles. This study shows that when *n*-dodecyl β-D-maltoside (DDM) is utilized as a dispersing and stabilizing agent in the synthesis and stabilization of poly[methyl methacrylate-*co*-(*n*-butyl acrylate)] (p-MMA/nBA) colloidal particles, stable colloidal dispersions can be formed. Since understanding of sugar−protein interactions have numerous practical and scientific implications, these studies examine DDM-stabilized p-MMA/nBA colloidal particles and their specific binding properties with concanavalin A (Con A). By use of spectroscopic analysis, unique binding characteristics that are a function of DDM concentration, time, and the concentration of Con A are detected. When DDM-stabilized p-MMA/nBA particles are allowed to coalesce, DDM is released from the particle surfaces and, under suitable conditions, selectively stratifies in the areas of the excess of interfacial energy near the film−air (F−A) interface, thus providing sites for attracting Con A via α-glucose−OH hydrogen bonding. Consequently, adsorption of Con A at the F−A interfaces occur and the degree of adsorption is controlled by the amount of DDM at the F−A interface.

Introduction

Recently, we reported[1] that the use of phospholipids during colloidal particle synthesis may generate films with stimuli-responsive characteristics. When such colloidal particles are allowed to coalesce, surface-localized ionic clusters (SLICs) with unique surface morphologies may be generated during film formation, leading to bioactive surfaces sensitive to pH, ionic strength, and other external stimuli.[2] As a result, unique rafts at the film−air (F−A) interfaces may be formed.[3,4] Expanding the scope of these findings, the use of sugars in the synthesis of colloids provides another avenue for creating polymeric films with bioactive properties.

Although sugars and their derivatives, which are common functional entities in biological systems, have been incorporated into polymeric materials in numerous applications,[5−12] including their use as polymeric surfactants[13] or polymerization stabilizing agents,[14,15] the first utilization of these species as colloidal dispersing agents was reported only recently.[16] Other studies involved the use of saccharide-functionalized polymer micelles to design polyvalent nanoscaffolds for the targeted drug delivery systems, which involved saccharide-functionalized polymers interactions with concanavalin A (Con A) and bacterial cell (*Escherichia coli*).[6,8] Since sugars are lyophilized with proteins, sugar−protein interactions provide stability for proteins during handling and storage stages.[11]

These studies focus on the formation of colloidal stimuli-responsive nanoparticles with sugar-modified surfaces, and of particular interest are interactions of these particles with Con A, which is a well-known plant lectin for in vitro biological activities arising from its specific saccharide-binding ability to α-glucose and α-mannose.[8−10,17] Combining colloidal particles stabilized by *n*-dodecyl β-D-maltoside (DDM) and sodium dioctyl sulfosuccinate (SDOSS) with Con A provides an opportunity for the development of biorecognizable surfaces sensitive to bonding to α-glucose moieties. Specifically, this study focuses on the development of biorecognition sites for Con A adsorption as well as understanding of interactions between Con A-coated surfaces and colloidal particles.

Experimental Section

Methyl methacrylate (MMA), *n*-butyl acrylate (nBA), *n*-dodecyl β-D-maltoside (DDM), sodium dioctyl sulfosuccinate (SDOSS), and potassium persulfate (KPS) were purchased from Aldrich Chemical Co. Concanavalin A (Con A) at a concentration of 5 mg/mL was purchased from Biomeda Co. Sodium chloride, sodium acetate, calcium chloride, and manganese(II) chloride were purchased from Aldrich Chemical Co., and Con A-coated polystyrene substrate (p-Sty/Con A) was purchased from Biomat Snc. (Italy).

MMA/nBA emulsion copolymer was synthesized by a semicontinuous process outlined elsewhere[18] and adapted for small-scale emulsion polymerization. The reaction flask was immersed in a water bath preheated to 74 °C and purged with N_2 gas. The reactor was charged with 10 mL of DDI water, and during N_2 purging for 30 min to remove oxygen, the content was stirred at 300 rpm. To enhance colloidal stability, relatively high concentration levels of DDM and SDOSS (5% w/w) of final solids content were utilized,[19] but the DDM/SDOSS ratios were varied from 0 to 10 wt % DDM out of the total surfactant content. MMA:nBA = 1/1 was added into the surfactants dissolved solution to make pre-emulsion with 41.95 wt % monomer concentration. After 30 min of N_2 purging, pre-emulsion and initiator solutions were fed at 0.333 and 0.095 mL/min into the vessel over a period of 3 and 3.5 h, respectively. After reaction was completed, bath temperature was raised to 80 °C while a 5 mL initiator chaser solution was added. The theoretical percent solids was 30.88%, and since no residual monomer was detected, this value represents the solid content of the solution. Upon cooling, the emulsion was filtered twice and the particle size analysis was performed on a Microtrac particle size analyzer model

* To whom correspondence should be addressed.

10.1021/bm050974p CCC: $33.50
Published on Web 03/04/2006

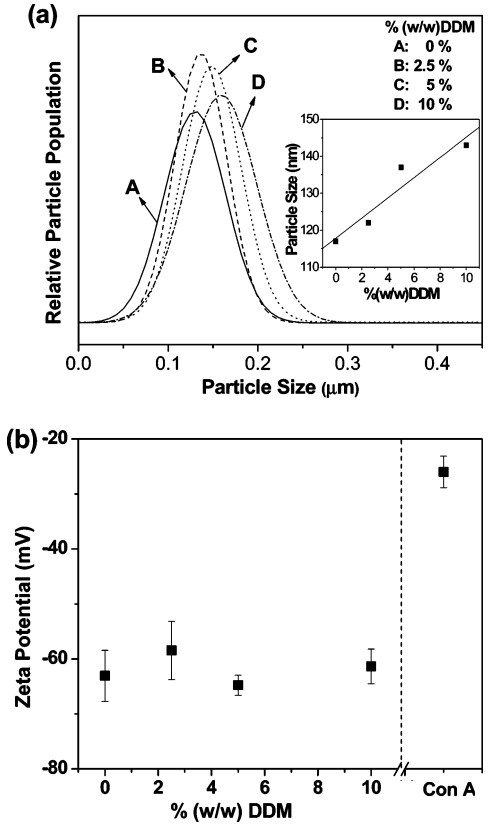

Figure 1. (a) Particle size analyses of dispersed colloidal particles of (A) p-MMA/nBA (0 wt % DDM), (B) p-MMA/nBA (2.5 wt % DDM), (C) p-MMA/nBA (5 wt % DDM), and (D) p-MMA/nBA (10 wt % DDM). **(**b**)** ζ potential recorded from prepared colloidal dispersions and Con A solution.

UPA250**.** Figure 1a illustrates particle size analysis of colloidal dispersions prepared with DDM as a dispersing agent. While trace A represents the particle size distribution for p-MMA/nBA without DDM with an average particle size of 117 nm, traces B, C, and D illustrate particle size distributions for p-MMA/nBA containing 2.5, 5, and 10 wt % DDM, respectively. As seen, as the concentration of DDM increases (while the total content of DDM/SDOSS remains constant), the particle size increases from 122 to 143 nm, and further increase of DDM above 10% (w/w) has no effect on the particle size, which remains at about 150 nm. Since particle interactions with Con A are of particular interest and the surface charges of individual particles, in particular in the presence of surface-active surfactants and proteins,[20−23] are responsible for these interactions, ζ potential measurements were conducted on a Malvern Zetasizer nano-ZS using diluted colloidal dispersion and Con A in DI water at room temperature. As illustrated in Figure 1a, the amount of DDM affects the particle size, but the ζ potential remains the same. This is illustrated in Figure 1b and indicates that the surface charge per particle surface area remain the same. In contrast, ζ potential value for Con A is significantly higher.

In an effort to verify binding properties between colloidal particles and Con A, colloidal dispersions prepared in the presence of DDM were mixed with Con A dissolved in 50 mM sodium acetate buffer solution (pH = 6.5, 0.9% sodium chloride containing 1 mM $[Ca^{2+}]$ and $[Mn^{2+}]$). Con A was diluted with sodium acetate buffer solution to give 0, 1.3×10^{-3}, 2.16×10^{-3}, 6.5×10^{-3}, and 1.3×10^{-2} g/L concentrations. It is essential that, in order to examine the effect of concentration, solution is prepared fresh before the experiment by adding *p*-MMA/nBA containing 10 wt % DDM to Con A buffer solution to maintain 1.3% (v/v), followed by stirring for 30 s before UV−vis measurements.

To determine the turbidity changes as a function of DDM/SDOSS ratio, 2.6×10^{-2} g/L Con A solution was prepared and mixed with 1.3% and 0.26% (v/v) p-MMA/nBA containing 10, 5, 2.5, and 0% (w/w) DDM, followed by stirring for 30 s. During turbidity analysis at the early stages (0−1 h), the first percent transmittance of diluted p-MMA/nBA (0.26% v/v) colloidal dispersion was collected and then Con A solution (2.6×10^{-2} g/L) was added and mixed quickly prior to second percent transmittance collection (collection cycle was once per 12 s). The p-MMA/nBA (0 wt % DDM) mixed with buffer solution was utilized to verify stability of colloidal dispersions in a buffer solution. The plots of turbidity changes (± 3.5%) were obtained by using Varian Cary 500 Scan UV−vis NIR spectrophotometer with 600 nm wavelength light at 25 °C.

Polymeric films were obtained by casting 0.5 mL of a colloidal dispersion onto a poly(tetrafluoroethylene) (PTFE) substrate to obtain film thickness of 300 μm. Aqueous colloidal dispersions of MMA/nBA copolymers containing a specific percentage of DDM were allowed to coalesce at 50% relative humidity (RH) and 30 °C for 5 days. Such coalesced films were immersed in Con A-diluted buffer solution (2.6×10^{-2} g/L) for 30 min and dried for 24 h in a desiccator. In an effort to study interaction between DDM and Con A, we conduct a series of model experiments. The relative volume of the DDM solution was added into 0.33 mL of Con A (5 mg/mL) solutions to obtain 1.29×10^{-2}, 1.88×10^{-2}, and 2.44×10^{-2} mol/L DDM in Con A solution, followed by stirring for 1 min. Such prepared solutions were cast onto a glass slide, followed by drying in the desiccator for 12 h. For analysis of particle interactions with Con A films, p-Sty/Con A films were immersed into diluted (1.3 vol %) p-MMA/nBA containing 10 wt % DDM and p-MMA/nBA without DDM colloidal dispersions for 10 s and dried for 24 h at 50% relative humidity (RH) and 30 °C for 24 h. To determine colloidal dispersion binding properties onto p-Sty/Con A, atomic force microscopy (AFM) images were collected on a Nanoscope IIIa Dimension 3000 scanning probe microscope (Digital Instruments) set at the resonance frequency of 310 kHz and tapping mode equipped with a Si probe (force constant = 40 N/m).

Attenuated total reflectance Fourier transform infrared (ATR FT-IR) spectra were collected on a Bio-Rad FTS-7000 FT-IR single-beam spectrometer set at 4 cm^{-1} resolution equipped with a mercury−cadmium−telluride (MCT) liquid nitrogen-cooled detector and a 45° face angle Ge crystal. Each spectrum represents 100 coadded scans ratioed against a reference spectrum obtained by recording 100 coadded scans of an empty ATR cell. All spectra were corrected for spectral distortion by use of Q-ATR software.[24]

Optical and internal reflection IR imaging (IRIRI) experiments[25] were conducted on a Digilab FTS 6000 Stingray imaging system with an internal reflection element (IRE). This system consists of a Digilab FTS 6000 spectrometer, a UMA 500 microscope, an ImagIR focal plane array (FPA) image detector, and a semispherical Ge IRE. IRIR images were collected with the following spectral acquisition parameters: undersampling ratio of 4, step-scan speed of 1 Hz, 1021 spectrometer steps, 160 images/step, and 8 cm^{-1} spectral resolution. In a typical experiment, spectral data set acquisition time was approximately 20 min. Image processing was performed with the Environment for Visualizing Images (ENVI) software (Research Systems, Inc., version 3.5). Appropriate baseline correction algorithms were applied to compensate for baseline deviations.

Results and Discussion

As stated in the Introduction, these studies focus on two aspects of Con A interactions with colloidal particles: (1) interactions of Con A and DDM-stabilized p-MMA/nBA colloidal particles in an aqueous phase and (2) interactions of Con A−polymer surfaces and Con A surface−p-MMA/nBA colloidal particle interactions.

(1) p-MMA/nBA Particles−Con A Solution Interactions. The first step in this investigation is to determine whether the α-glucose moiety of DDM of the colloidal p-MMA/nBA dispersions exhibits affinity toward Con A. This is accomplished by monitoring kinetics of the binding activity after addition of

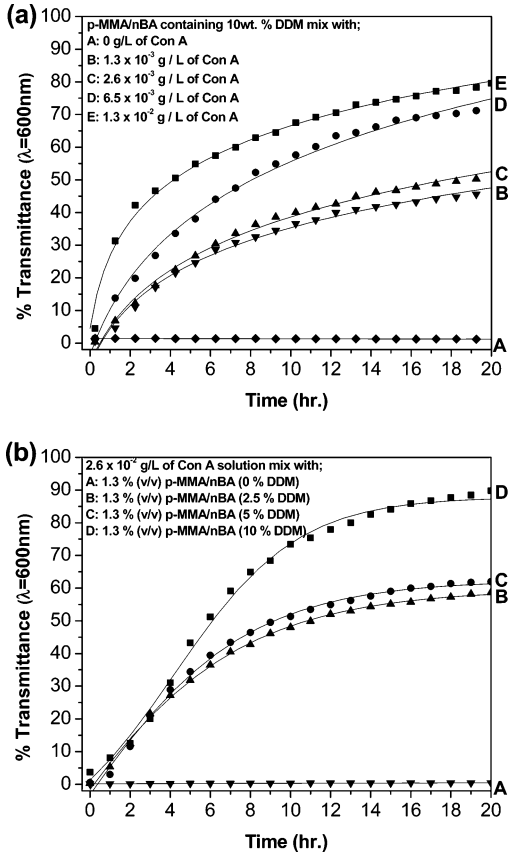

Figure 2. UV−Vis spectroscopy percent transmittance plots as a function of time for the rate of turbidity changes **(**a) by adding various concentrations such as (A) 0, (B) 1.3×10^{-3}, (C) 2.6×10^{-3}, (D) 6.5×10^{-3}, and (E) 1.3×10^{-2} g/L Con A into diluted (1.3% v/v) p-MMA/nBA containing 10 wt % DDM, or (b**)** by adding a certain concentration (2.6×10^{-2} g/L) of Con A into diluted (1.3% v/v) p-MMA/nBA with (A) 0, (B) 2.5, (C) 5, and (D) 10 wt % DDM (an error of less than 7%).

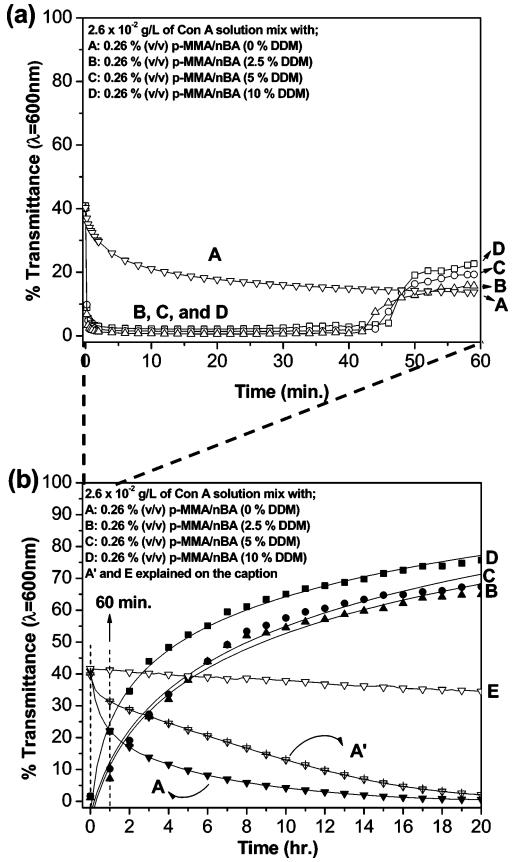

Figure 3. UV−Vis spectroscopy percent transmittance plots as a function of time for the rate of turbidity changes by adding a certain concentration (2.6×10^{-2} g/L) of Con A into diluted (0.26% v/v) p-MMA/nBA with (A) 0, (B) 2.5, (C) 5, and (D) 10 wt % DDM. **(**a) Initial percent transmittance changes in the range from 0 to 1 h; (b) entire 20 h time course of panel a. Traces A′ and E shows turbidity changes of diluted (0.26% v/v) p-MMA/nBA (0 wt % DDM) by adding different concentrations of Con A (2.6×10^{-3} and 0 g/L, respectively).

Con A to respective colloidal dispersions stabilized by various amounts of DDM. Since the particle−Con A binding causes precipitation of these species, measuring the percent transmittance of the solution changes will provide us with a quantitative measure of the degree of precipitation of colloidal particles as a function of time. Figure 2a illustrates the percent transmittance changes of the 600 nm UV−vis band plotted as a function of time for diluted (1.3% v/v) p-MMA/nBA (10 wt % DDM) solutions containing various concentration levels of Con A at sodium acetate buffer solution (pH 6.5). As seen in curve A, the percent transmittance of colloidal dispersions does not change after 20 h, thus indicating an excellent stability of colloidal dispersions in the buffer solution. However, upon addition of Con A, the percent transmittance increases as a function of Con A concentration, indicating that the presence of Con A results in the precipitation of colloidal particles. As seen in curve B, the percent transmittance of diluted colloidal dispersions in the presence of 1.3×10^{-3} g/L Con A increases as a function of time. Furthermore, the rate of percent transmittance increases with the increased concentration levels of Con A. This is depicted in curves B−E of Figure 2a, demonstrating that the increased transmittance results from the precipitation of colloidal particles, which is proportional to the concentration levels of Con A.

With these measurements in mind, let us consider the binding efficiency of Con A to p-MMA/nBA as a function of concentration of DDM on the surface of p-MMA/nBA particles. Figure 2b illustrates the rate of precipitation measured again by the percent transmittance changes of diluted p-MMA/nBA (1.3% v/v) solutions containing 0, 2.5, 5, and 10 wt % DDM in the presence of an excess amount (2.6×10^{-2} g/L) of Con A. These conditions ensure that all DDM sites on colloidal particles will have an opportunity to be occupied by Con A, if indeed Con A−p-MMA/nBA interactions are responsible for the particle precipitation. As seen in curve A, the percent transmittance of p-MMA/nBA without DDM exhibits no change over the period of 20 h, but significant increase is detected for p-MMA/nBA particles containing 2.5, 5, and 10 wt % DDM. These results further substantiate the fact that colloidal particles precipitate when DDM is used as the dispersing agent, and furthermore, the rate of precipitation increases for higher concentration levels of DDM on p-MMA/nBA particles, which is illustrated in curves B−D in Figure 2b. Colloidal dispersions with 30 and 50 wt % DDM exhibit similar percent transmittance changes than that observed for curve D, thus implying that the rate of precipitation remains the same when the DDM/SDOSS ratio is greater than 1/9.

The effect of particle concentration was also examined. Figure 3a illustrates the first 60 min of the percent transmittance changes as a function of time for 0.26% (v/v) p-MMA/nBA particles, and Figure 3b shows the entire 20 h. As shown in Figure 3a, for the particles without DDM, the percent transmittance is diminished, indicating that coagulation occurs between colloidal particles and Con A. However, no precipitation is observed even after 20 h, as demonstrated by curve A in Figure

3b. In contrast, for colloidal dispersions containing DDM a drastic drop of the percent transmittance is observed upon addition of Con A, followed by the increase after 40 min. This is shown in curves B−D. These observations indicate significant binding between the colloidal particles and Con A. As noted earlier, diminished percent transmittance for particles without DDM is observed, which is believed to be attributed to heterocoagulation, and the size and the particle charges are the primary forces. Indeed, small particles tend to heterocoagulate with larger particles, even if they exhibit the same surface charges.[19] Since Con A is about 10-fold smaller than the colloidal particles and has ability to attract large cations,[26] as demonstrated by the ζ potential differences shown in Figure 1b, heterocoagulation leading to the percent transmittance decreases as a function of time, as observed in curve A of Figure 3. Furthermore, lower concentration levels of Con A shown in curve A′ result in the diminished rates of percent transmittance in time, indicating concentration-dependent heterocoagulation. For the reference, a plot of the percent transmittance for p-MMA/nBA (0% DDM) in the buffer solution shows no changes, as shown by curve E of Figure 3b.

In summary, two concurrent phenomena occur for colloidal solutions containing p-MMA/nBA and Con A: (1) selective binding between α-glucose moieties of p-MMA/nBA particles through DDM and Con A and (2) heterocoagulation resulting from the interactions between p-MMA/nBA and Con A. To further confirm that indeed Con A is consumed by precipitation with p-MMA/nBA particles, the 275 nm band due to $\pi \rightarrow \pi^*$ transitions of Con A also diminishes with time (not shown),[27,28] thus indicating again the precipitation of Con A resulting from the aggregation with p-MMA/nBA particles.

(2) Film−Particle Interactions. In an effort to determine the nature of interaction between coalesced films and Con A, p-MMA/nBA colloidal dispersions containing 0, 2.5, 5, and 10 wt % DDM were allowed to coalesce. Such films were immersed into Con A diluted buffer solution, and ATR FT-IR analysis of polymeric films was performed. Figure 4a illustrates ATR FT-IR spectra recorded from the film−air (F−A) and film−substrate (F−S) interfaces of the coalesced films with and without 10% DDM. As shown in Figure 4a, upon exposure to Con A solution of the F−A and F−S interfaces, amide I bands[29] due to Con A are detected in the 1700−1500 cm^{-1} regions. While traces A and A′ illustrate ATR FT-IR spectra recorded from the F−A and F−S interfaces of p-MMA/nBA films containing 10 wt % DDM, respectively, traces B and B′ were recorded from the F−A and F−S interfaces of p-MMA/nBA films without DDM. As seen, binding of Con A at the F−A of p-MMA/nBA containing 10 wt % DDM (trace A) is manifested by higher intensity at the 1635 cm^{-1} band (amide I). In contrast, in trace A′ this band is weak, indicating that DDM migrates to the F−A interface during film formation,[16] which facilitates binding with Con A. As seen in traces B and B′, Con A still exhibits the same affinity toward the F−A and F−S interfaces of p-MMA/nBA films without DDM, but the degree of association is small, which is likely attributed to heterocoagulation between the surface and Con A. For reference purposes, trace C illustrates ATR FT-IR spectra of p-MMA/nBA exposed to sodium acetate buffer solution without Con A. Similar experiments were performed for different concentration levels of DDM, and the band intensities of Con A become weaker as lower concentration levels of DDM in p-MMA/nBA colloidal dispersions are utilized. This is shown in Figure 4b.

Although the above data show that the presence of Con A causes precipitation of DDM-stabilized p-MMA/nBA dispersions, to identify the nature of the interactions between DDM and Con A, we conducted a series of model experiments where DDM and Con A solutions were cast onto a glass slide to form a film. As seen in Figure 5, traces A and E are the reference spectra of Con A and DDM, respectively, and traces B−D represent the spectra collected from Con A/DDM films. As shown in Figure 5a, the bands due to amide I and amide II are of particular interest, as these entities are responsible for the interactions between Con A and DDM. The band at 1635 cm^{-1} in traces A−D represent hydrogen-bonded C═O stretching vibrations (amide I), while the broad band at 1650 cm^{-1} is due to free amide I of Con A. As shown, addition of DDM results in lower intensity of the free amide I bands while the hydrogen-bonded amide I band exhibits no changes. At the same time, two bands at 1536 and 1519 cm^{-1} due to hydrogen-bonded amide II and free amide II band (NH deformation vibrating), respectively, decrease as the amount of DDM increases (traces A−D in Figure 5b). In particular, free amide II band at 1519 cm^{-1} decreases rapidly for the same conditions, thus indicating that amide I and amide II of Con A are responsible for binding with DDM via hydrogen bonding between the hydroxyl groups of DDM and the amide groups of Con A.

In an effort to identify whether Con A adsorption is uniform, optical and IRIR images from the F−A interface were recorded. Figure 6a,b illustrates optical and IR images after Con A was allowed to be affixed onto the F−A interface of p-MMA/nBA films containing 10 wt % DDM. As demonstrated by the optical

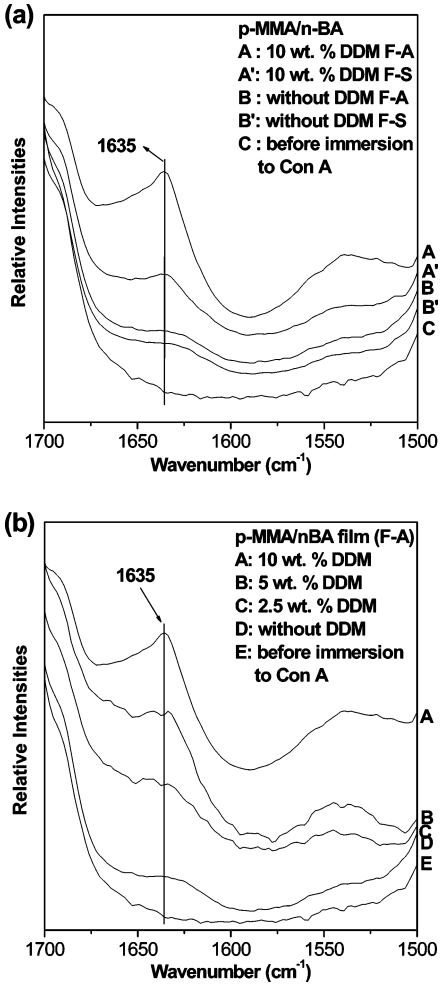

Figure 4. ATR FT-IR spectra recorded from Con A-bound (a) F−A and F−S interfaces of p-MMA/nBA coalesced films containing 10 and 0 wt % DDM and (b) F−A interfaces of p-MMA/nBA containing 10, 5, 2.5, and 0 wt % DDM films.

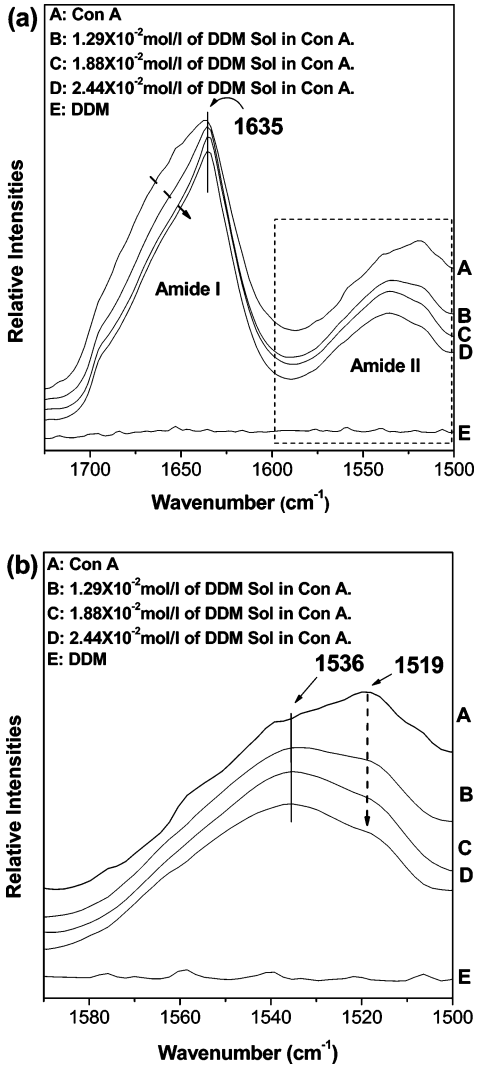

Figure 5. (a) ATR FT-IR spectroscopy recorded from dried samples of (A) Con A; (B) 1.29 × 10^{-2}, (C) 1.88 × 10^{-2}, and (D) 2.44 × 10^{-2} mol/L DDM solution in Con A; and (E) DDM (E). **(b)** ATR FT-IR spectra of inset in panel a.

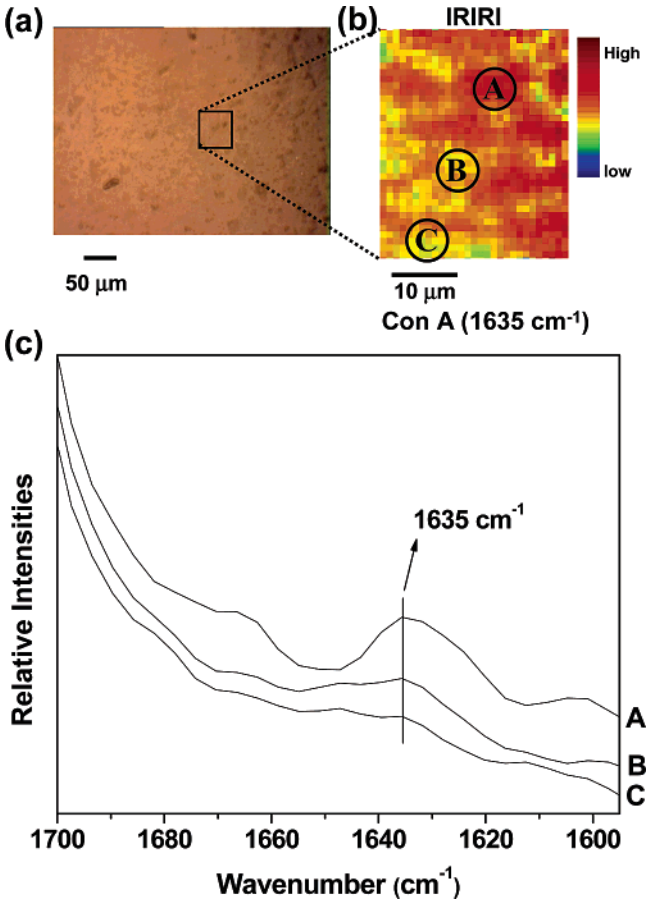

Figure 6. (a) Optical images for the Con A-bound F−A interface of p-MMA/nBA coalesced films containing 10 wt % DDM films. **(**b) IRIR image collected from the specified regions of optical images. (c) IR spectra recorded from areas labeled A, B, and C in the IRIR image.

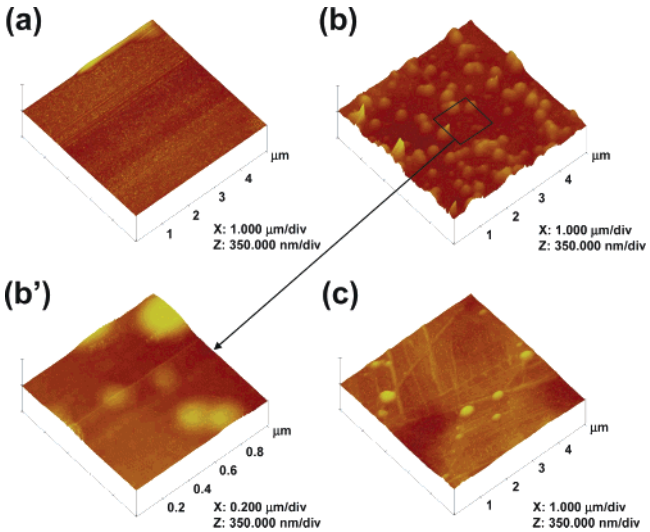

Figure 7. Topographic atomic force microscopy (AFM) images collected from **(**a) Con A−Sty surface (*x* axis = 5 μm), (b) Con A−Sty surface exposed to p-MMA/nBA (10 wt % DDM) colloidal particle solution, (b′) enlarged image recorded form marked area of image b (*x* axis = 1 μm), and (c) p-MMA/nBA (without DDM) colloidal particle binding on the Con A−Sty surface.

image, the adsorption is not homogeneous, which is also confirmed by IRIR images (Figure 6b). As seen in Figure 6c, IR spectra recorded from areas A, B, and C illustrate higher concentration levels of Con A in area A, which is manifested by the higher intensity of the 1635 cm^{-1} band.

Surface morphological features resulting from Con A−DDM interactions are illustrated in Figure 7, which shows AFM images recorded from the p-Sty/Con A surface (a) and surfaces treated with the diluted (1.3% v/v) p-MMA/nBA containing 10 wt % DDM (b) and p-MMA/nBA without DDM solution (c). As seen, p-Sty/Con A surface is flat and clear, thus providing optimum conditions for monitoring surface topology changes. In contrast, Figure 7b shows an AFM image of the p-Sty/Con A film immersed in p-MMA/nBA colloidal solution in which p-MMA/nBA particles were stabilized by 10% DDM. As seen, p-MMA/nBA particles are selectively attached to the surface, and Figure 7b′ is the magnified image of the inset square area marked in Figure 7b which indeed show single colloidal particles attached to the surface, as demonstrated by their distorted spherical shapes. To compare these images to the images obtained from p-Sty/Con A surfaces exposed to p-MMA/nBA but containing no DDM, the AFM image shown in Figure 7c was collected. As seen, occasionally, there is particle adsorption at the surface, but concentration levels are extremely low. Also, the shape of the p-MMA/nBA particles without DDM is almost perfectly spherical, suggesting some degree of heterocoagulation.

Based on spectroscopic and morphological data presented above, mechanisms responsible for interaction between p-MMA/nBA particles are proposed and schematically illustrated in

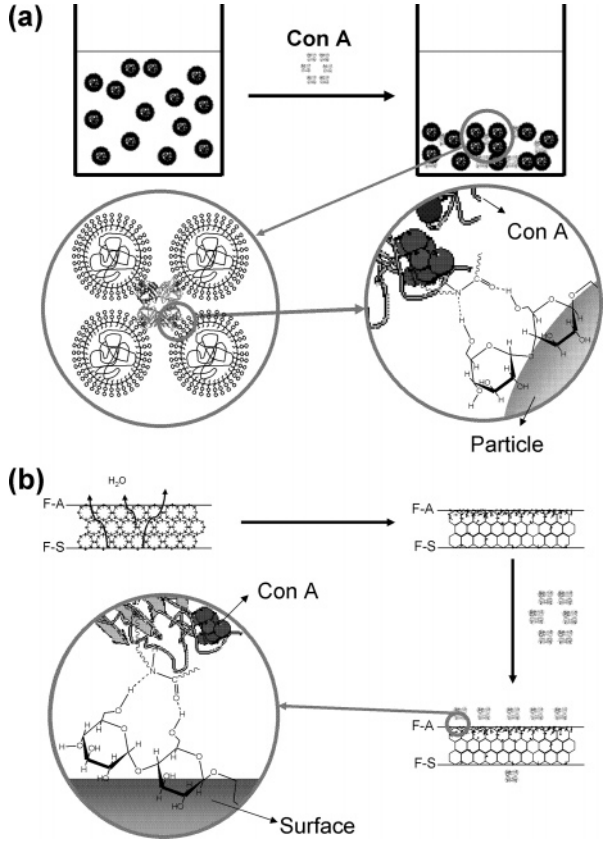

Figure 8. Schematic representation of (a) interactions between Con A and DDM-−stabilized colloidal particles in aqueous solution; (b) coalesced p-MMA/nBA film−Con A interactions.

Figure 8. As shown in Figure 8a, previously dispersed colloidal dispersions precipitate out of the solution as a result of interactions with Con A caused by interactions between α-glucose of DDM on the surface of p-MMA/nBA particles and Con A. The mechanisms responsible for these interactions are α-linkages of glucose and hydroxyl groups of DDM that facilitate hydrogen bonding with the amide group of Con A. Spectroscopic evidence was provided in Figure 5. For coalesced films, DDM stratification at the F−A interface during coalescence generates DDM-rich environments and facilitates bonding of Con A to this interface. This is illustrated in Figure 8b, and H-bonding is responsible for Con A−film interactions, which again are facilitated by the presence of DDM in the interfacial regions.

Conclusion

These studies showed that when DDM serves as dispersing species during colloidal synthesis of p-MMA/nBA as well as the stabilizing agent of colloidal dispersions, its presence significantly affects interactions between particles of p-MMA/nBA and Con A. Due to the presence of α-glucose moieties, which exhibit specific affinity toward Con A, p-MMA/nBA particles precipitate out and the degree of precipitation is directly related to the DDM content. When p-MMA/nBA coalesces, DDM is released from the particle surfaces and, under suitable conditions, selectively stratifies in the areas of excess interfacial energy near the F−A interface. Such interface also attracts Con A via α-glucose−OH group hydrogen-bonding interactions, resulting in adsorption of Con A at the F−A interface. These studies also show that protein adsorption on colloidal particles as well as on polymeric films can be controlled by the content of DDM, which serves as a recognition site for selective protein adsorption.

Acknowledgment. This work was supported primarily by the MRSEC Program of the National Science Foundation under award DMR 0213883.

References and Notes

(1) Yacoub, A.; Urban, M. W. *Biomacromolecules* **2003**, *4* (1), 52−56.
(2) Lestage, D. J.; Schleis, D. J.; Urban, M. W. *Langmuir* **2004**, *20* (17), 7027−7035.
(3) Zhao, Y.; Urban, M. W. *Macromolecules* **2000**, *33* (22), 8426−8434.
(4) Dreher, W. R.; Urban, M. W.; Porzio, R. S.; Zhao, C. L. *Langmuir* **2003**, *19* (24), 10254−10259.
(5) Dedinaite, A.; Bastardo, L. *Langmuir* **2002**, *18* (24), 9383−9392.
(6) Joralemon, M. J.; Murthy, K. S.; Remsen, E. E.; Becker, M. L.; Wooley, K. L. *Biomacromolecules* **2004**, *5* (3), 903−913.
(7) Lipatova, T. E.; Pkhakadze, G. A.; Snegirev, A. I.; Vorona, V. V.; Shilov, V. V. *J. Biomed. Mater. Res.* **1984**, *18* (2), 129−36.
(8) Serizawa, T.; Yasunaga, S.; Akashi, M. *Biomacromolecules* **2001**, *2* (2), 469−475.
(9) Sugiyama, K.; Kato, K.; Kido, M.; Shiraishi, K.; Ohga, K.; Okada, K.; Matsuo, O. *Macromol. Chem. Phys.* **1998**, *199* (6), 1201−1208.
(10) Sugiyama, K.; Oku, T. *Polym. J.* **1995**, *27* (2), 179−88.
(11) Taylor, L. S.; Zografi, G. *J. Pharm. Sci.* **1998**, *87* (12), 1615−1621.
(12) Yoshizumi, A.; Kanayama, N.; Maehara, Y.; Ide, M.; Kitano, H. *Langmuir* **1999**, *15* (2), 482−488.
(13) Esquena, J.; Dominguez, F. J.; Solans, C.; Levecke, B.; Booten, K.; Tadros, T. F. *Langmuir* **2003**, *19* (25), 10463−10467.
(14) Marie, E.; Landfester, K.; Antonietti, M. *Biomacromolecules* **2002**, *3* (3), 475−481.
(15) Castro, L. B. R.; Soares, K. V.; Naves, A. F.; Carmona-Ribeiro, A. M.; Petri, D. F. S. *Ind. Eng. Chem. Res.* **2004**, *43* (24), 7774−7779.
(16) Bae, W.-S.; Lestage, D. J.; Proia, M.; Heinhorst, S.; Urban, M. W. *Biomacromolecules* **2005**, *6*, 2615−2621.
(17) Sherry, A. D.; Buck, A. E.; Peterson, C. A. *Biochemistry* **1978**, *17*, 2169−73.
(18) Davis, S. D.; Hadgraft, J.; Palin, K. J. *Encylopedia of Emulsion Technology*; Marcel Dekker: New York, 1985; Vol. 2.
(19) Lovell, P. A.; El-Aasser, M. S., *Emulsion polymerization and emulsion polymers*; John Wiley & Sons Ltd.: West Sussex, England, 1997.
(20) Awad, D.; Tabod, I.; Lutz, S.; Wessolowski, H.; Gabel, D. *J. Organomet. Chem.* **2005**, *690* (11), 2732−2735.
(21) McNamee, C. E.; Matsumoto, M.; Hartley, P. G.; Mulvaney, P.; Tsujii, Y.; Nakahara, M. *Langmuir* **2001**, *17* (20), 6220−6227.
(22) Ruso, J. M.; Attwood, D.; Garcia, M.; Prieto, G.; Sarmiento, F.; Taboada, P.; Varela, L. M.; Mosquera, V. *Langmuir* **2000**, *16* (26), 10449−10455.
(23) Prieto, G.; Sabin, J.; Ruso, J. M.; Gonzalez-Perez, A.; Sarmiento, F. *Colloids Surf., A* **2004**, *249* (1−3), 51−55.
(24) Huang, J. B.; Urban, M. W. *Appl. Spectrosc.* **1992**, *46* (11), 1666−72.
(25) Otts, D. B.; Zhang, P.; Urban, M. W. *Langmuir* **2002**, *18* (17), 6473−6477.
(26) Parkin, S.; Rupp, B.; Hope, H. *Acta Crystallogr.* **1996**, *D52* (6), 1161−1168.
(27) Cardin, A. D.; Behnke, W. D.; Mandel, F. *J. Biol. Chem.* **1979**, *254* (18), 8877−84.
(28) Matsumoto, I.; Uehara, Y.; Jimbo, A.; Seno, N. *J. Biochem. (Tokyo)* **1983**, *93* (3), 763−9.
(29) van de Weert, M.; Haris, P. I.; Hennink, W. E.; Crommelin, D. J. A. *Anal. Biochem.* **2001**, *297* (2), 160−169.

BM050974P